Available online at www.sciencedirect.com
SCIENCE DIRECT®
Journal of Inorganic Biochemistry 99 (2005) 415–423
JOURNAL OF Inorganic Biochemistry
www.elsevier.com/locate/jinorgbio

Single crystal EPR study of electronic structure and exchange interactions for copper(II)(L-arginine)$_2$(SO$_4$) · (H$_2$O)$_6$: a model system to study exchange interactions between unpaired spins in proteins

R.C. Santana [a,*], R.O. Cunha [a], J.F. Carvalho [a], I. Vencato [a], R. Calvo [b]

[a] *Universidade Federal de Goiás, Instituto de Física, CP 131, Goiânia, Goiás, 74001-970, Brazil*
[b] *Departamento de Física, Facultad de Bioquímica y Ciencias Biológicas, Universidad Nacional del Litoral and INTEC (CONICET–UNL), Güemes 3450, 3000 Santa Fe, Argentina*

Received 19 August 2004; received in revised form 4 October 2004; accepted 13 October 2004

Abstract

We report EPR measurements at 9.77 and 34.1 GHz in powder and single crystal samples of the ternary copper amino acid complex Cu(L-arginine)$_2$(SO$_4$) · (H$_2$O)$_6$. The single crystal Electron Paramagnetic Resonance spectra display a single resonance for all magnetic field orientations in the *ca* and *cb* crystal planes. In the *ab* plane they display two resonances for most orientations of the magnetic field, and only one resonance for orientations close to the crystal axes. This behavior is a result of the selective collapse of the resonances corresponding to the four copper sites in the unit cell produced by the exchange interactions between copper ions. From the characteristics of the collapse and the angular dependences of the position and width of the resonances we evaluate the *g*-tensors of the copper molecules and estimate exchange interactions $|J_1/k_B| = 0.9$ K and $|J_2/k_B| = 0.009$ K between copper neighbors at 5.908 Å and at 15.684 Å, respectively. J_1 is assigned to a *syn–anti* equatorial–apical carboxylate bridge with a total bond length of 7.133 Å. J_2 is assigned to a long bridge of 12 atoms with a total bond length of 19.789 Å, that includes two hydrogen bonds. The results are discussed in terms of the crystal and electronic structure of Cu(L-arginine)$_2$(SO$_4$) · (H$_2$O)$_6$. We show that J_2 is in excellent agreement with the observed magnetic interaction between the reduced quinone acceptors in the photosynthetic reaction center protein of the bacterium *Rb. sphaeroides*, which is transmitted along a similar chemical path containing two hydrogen bonds. Our findings indicate that it is valid to estimate values for the exchange interactions between redox centers in proteins transmitted along long chemical paths containing sigma and H-bonds, from data obtained in model systems, and emphasize the importance of measuring exchange interactions in biologically relevant model systems.

Keywords: EPR spectroscopy; Exchange interaction; Copper complexes; Model systems; Biomolecules

1. Introduction

The important role of weak non covalent interactions in the structure and behavior of biological macromolecules is well recognized [1]. They contribute to the structure, optimize molecular reactivity, allow molecular recognition, and more. In electron transfer proteins, long chemical paths are conveniently tuned to regulate the kinetics of the transfer process, and thus the function of the protein.

The best known and most important weak interactions between metal ions, radicals or redox centers con-

* Corresponding author. Tel./fax: +55 62 521 1029.
E-mail address: santana@if.ufg.br (R.C. Santana).

0162-0134/$ - see front matter © 2004 Elsevier Inc. All rights reserved.
doi:10.1016/j.jinorgbio.2004.10.014

tain H-bonds [2,3]. Aromatic rings provide various other types of weak couplings like ring stacking [4,5], cation-π [6,7], NH–π [8], and CH–π interactions [9]. Real chemical paths are usually a sequence of some of these elemental weak interactions plus other strong covalent bonds. They may be identified in protein structure databases, and reproduced in model systems.

A convenient way to characterize a chemical path connecting two unpaired electrons is to evaluate the exchange interaction transmitted through the diamagnetic path connecting the spins (often called superexchange). The underlying principles of this interaction have been well described in the literature [10] and its magnitude is strongly dependent of the electronic structure of the path. Also, it has been shown that the matrix element for electron transfer between redox centers is related to the magnitude of the exchange interaction transmitted through the path [11–14].

The electron paramagnetic resonance (EPR) spectra of metal ions (e.g., copper) is useful to investigate local properties of a compound in the neighborhood of the metal [15]. In addition, weak exchange interactions (J) transmitted through long chemical paths bridging the unpaired spins (up to ~30 Å) can be evaluated by EPR [16–18]. Thus, EPR measurements contribute useful information to study the electronic structure of metal ions and the chemical paths connecting them. In fact EPR measurements in single crystal samples is the most powerful technique to evaluate selectively very weak exchange interactions, even in the presence of much stronger contributions [16–18].

Important model systems to study weak interactions are metal derivatives of amino acids [19]. The metal ions, often bonded through the amino and carboxylato groups, are important in the structure of the individual molecules. The functional groups of the amino acids provide a large variety of possibilities for weak bonding within and between molecules in the solid state [20]. In addition, ternary complexes including an amino acid or peptide, a metal ion, and a small inorganic or organic molecule, provide additional possibilities of modeling [21,22].

In recent years Yamauchi and collaborators [20–24] have reported interesting results about the structure, stability, self-organization and supramolecular associations of several binary and ternary copper compounds of arginine. These properties, produced by the coordination of the metal–ion and the interplay of various noncovalent interactions, are strongly influenced by the characteristics of the guanidinium group of arginine, a binding site for H-bonds, and by the various additional ligands which have been added to the compounds.

The compound Cu[L-arginine]$_2$(SO$_4$) · (H$_2$O)$_6$ [C$_{12}$H$_{40}$N$_8$O$_{14}$CuS], hereafter called Cu(L-arg)$_2$SO$_4$, whose structure was reported recently by Ohata et al. [22], shows self organization and structure-determining factors typical of ternary compounds of copper with arginine. These authors [22] also reported EPR data in solution and in the solid state (powder samples), and circular dichroism measurements. From their EPR data Ohata et al. [22] concluded that the copper ions are in a crystal field of tetragonal symmetry with a $d(x^2 - y^2)$ orbital ground state. However, due to the nature of the samples, their EPR results did not allow to obtain information about the spin–spin interactions, that are important to characterize chemical paths.

The compound Cu(L-arg)$_2$SO$_4$ is reanalyzed here through detailed EPR measurements in single crystals. These data allow us to evaluate exchange interactions between copper ions connected by long chemical paths containing H-bonds, and to discuss the results in terms of the structure of the paths. Our magneto-structural findings in Cu(L-arg)$_2$SO$_4$ are compared with recently reported values of the interaction between the reduced quinone acceptors in the biradical $Q_A^- Q_B^-$ in the photosynthetic reaction center protein from the bacterium *Rb. Sphaeroides* [13a,b].

2. Experimental

2.1. Sample preparation

The amino acid L-arginine, obtained from Ajinomoto Co, was used without further purification. The compound Cu(L-arg)$_2$SO$_4$ was obtained as described by Ohata et al. [22] from the reaction of L-arginine (0.348 g, 2.0 mmol) with CuSO$_4$ · 5H$_2$O in water (0.270 g, 1.0 mmol). The pH of the resulting solution was adjusted to 4.35, and the solution was left to evaporate at room temperature. Blue rectangular prismatic crystals elongated along the c-axis grew from the solution in few days. Powder X-ray diffraction measurements were performed to identify the obtained material as that studied by Ohata et al. [22]. Thus, we analyze our experimental results using the complete structural data tables deposited by these authors at the Cambridge Crystallographic Data Centre under number 137772.

Orientation of the single crystal samples for the EPR experiments was attained by gluing a (0 1 0) growth face of the sample to a cubic piece of KBr single crystal holder obtained by cleavage. This holder defines a set of orthogonal axes x, y, z; the a, b and c crystal axes of the orthorhombic single crystal were positioned along the x, y and z axes of the holder, respectively.

2.2. EPR measurements

We used a Bruker ESP–300 EPR spectrometer working at 9.77 (X-band) and at 34.1 GHz (Q-band), stand-

ard Bruker cavities operating with 100 kHz magnetic field modulation, and a rotating magnet. The magnetic field (B) was calibrated using diphenylpicrylhydrazyl (DPPH) positioned close to the sample as a field marker ($g = 2.0036$).

EPR spectra ($d\chi''/dB$) from powdered material and from oriented single crystals were collected digitally at room temperature. Spectra of powder samples at X and Q bands (data not shown) are useful as fingerprints of the material. They show no resolved hyperfine structure, as expected in the presence of exchange interactions between the copper ions.

The single crystal spectra were obtained at 5° intervals in three orthogonal planes (*ab*, *ca* and *cb*), in a range of 180°. A single resonance line without hyperfine splitting was observed for all orientations of the magnetic field $\boldsymbol{B}$ in the *ac* and *bc* planes. Two resonances were observed for $\boldsymbol{B}$ in the *ab* plane, except in directions close to the crystal axes, where they collapse to a single resonance. The position and peak-to-peak line width ΔB_{pp} of the single resonance, or the two resonances in some orientations of the *ab* plane, were obtained by least-squares fits of the field derivative of one or two Lorentzian line shapes to the observed signal. Fig. 1 shows a typical single crystal EPR spectrum obtained at 34.1 GHz with $\boldsymbol{B}$ in the *ab* plane, and includes the decomposition of the observed spectrum in two individual resonances. Good agreement was obtained between fitted and observed spectra. These fits provide the squared *g*-factor and the line width of the resonances (one in the *ac* and *bc* planes, and two in the *ab* plane) whose angular variations at Q-band are displayed in Figs. 2 and 3, respectively. Similar results were obtained at X-band (data not shown).

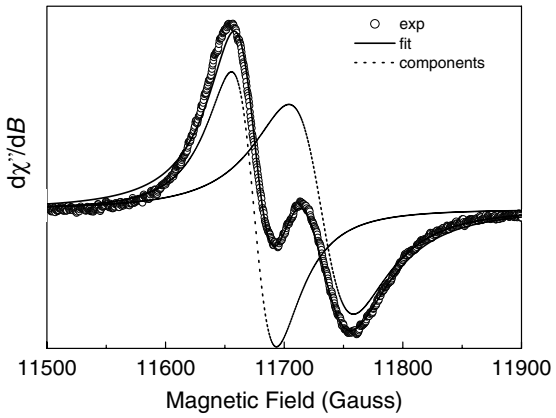

Fig. 1. Typical EPR spectra observed with the magnetic field at 45° from the *a* axis in the *ab* plane. Open circles are the experimental data at 34.1 GHz. The solid line was obtained fitting the sum of two Lorentzian lines to the experimental result. The dashed lines represent the two components of the fit.

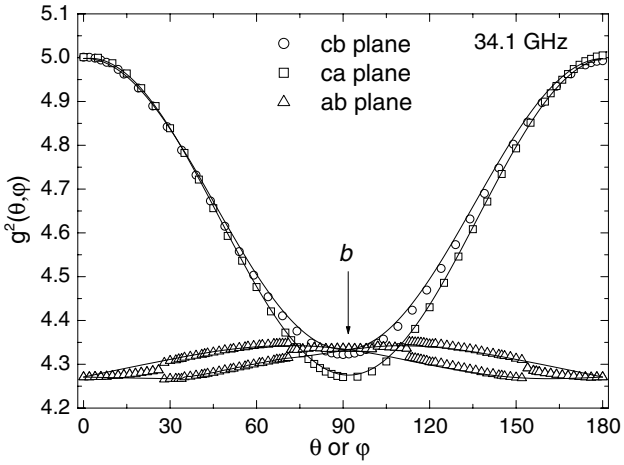

Fig. 2. Angular variation of $g^2(\theta,\varphi)$ at 34.1 GHz for the magnetic field applied in the *ab*, *ca* and *cb* crystalline planes of Cu(L-arg)$_2$SO$_4$. The solid lines are calculated with the values of the components of g^2 included in Table 2.

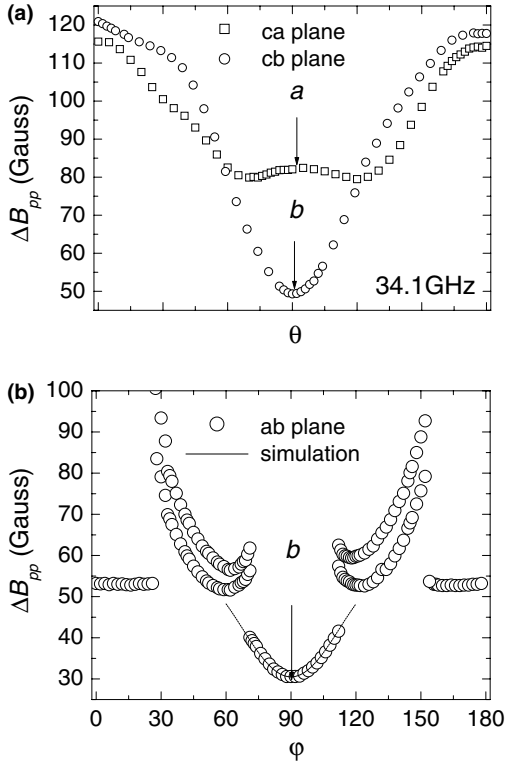

Fig. 3. Angular variation of the peak-to-peak line width ΔB_{pp} measured at 34.1 GHz in the (a) *ca* and *cb* planes, and (b) *ab* plane of a Cu(L-arg)$_2$SO$_4$ single crystal. The solid line in the angular region near to the *b* axis was obtained with the model described in the text, and gives information about the exchange coupling.

3. Crystal structure and exchange pathways for Cu(L-arg)$_2$SO$_4$

Cu(L-arg)$_2$SO$_4$ is orthorhombic, space group $P2_12_12_1$ with $Z = 4$ and lattice parameters $a = 13.152$ Å,

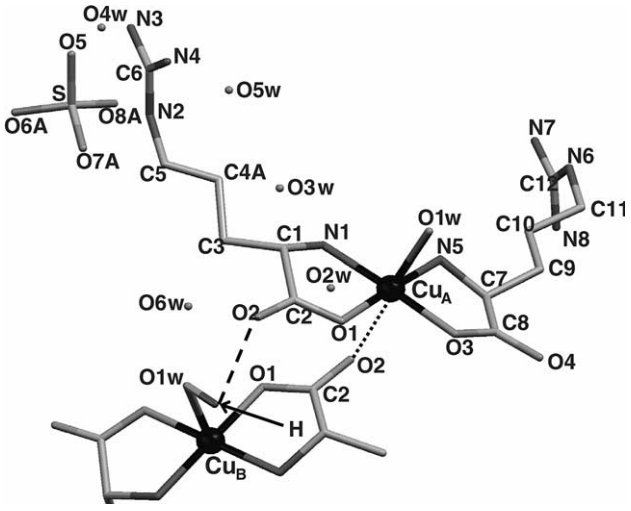

Fig. 4. Molecular structure of Cu(L-arg)$_2$SO$_4$ showing the chemical path connecting Cu$_A$ to Cu$_B$. The labeling of the atoms used is that from the Cambridge Structural Database, different from that used in [22]. Dashed and dot lines indicates, respectively, H and weak structural bonds. Hydrogen atoms were omitted for clarity.

b = 27.044 Å, and c = 7.321 Å [22]. The copper ion, *cis*-coordinated to two L-arginine molecules, is displaced 0.05 Å out of the plane of an approximately square N_2O_2 array (see Fig. 4, obtained from the crystallographic data of Ohata et al. [22]). The average distance to the carboxylate oxygens O1 and O3 is d(Cu–O) = 1.950 Å, and to the nitrogens N1 and N5 of amino groups of arginine molecules is d(Cu–N) = 1.978 Å. In the axial direction there is one oxygen atom O1w from a water molecule at d(Cu–O1w) = 2.461 Å. A sixth octahedral position, occupied by O2 from a neighboring L-arginine molecule, considered as a weak structural bond due to its relatively short length (d = 2.697 Å), completes a square bipyramid. The 3D arrangement of the molecules in Cu(L-arg)$_2$SO$_4$ gives rise to infinite right handed 1D single-helical chains with double strand along the a axis [22]. The four symmetry related copper molecules in the unit cell of Cu(L-arg)$_2$SO$_4$, labeled as A ≡ (x, y, z), B ≡ (1/2 − x, –y, 1/2 + z), C ≡ (−x, 1/2 + y, 1/2 − z) and D ≡ (1/2 + x, 1/2 − y, –z) [25] are chemically identical, but magnetically nonequivalent in the presence of a magnetic field. Molecules B, C and D are obtained from molecule A by 180° rotations around the crystallographic axes c, b and a, respectively, plus a translation.

Hydrogen bonds play an important role in the structure of Cu(L-arg)$_2$SO$_4$ and are key factors in the properties of the chemical paths we want to characterize. Thus, we summarize in Table 1 the properties of the H-bonds important for our purpose. The distances and angles are taken from the structural study of Ohata et al. [22]; using these values and the results of Steiner [26], we classify these bonds in the last column of Table 1 as weak, "w", moderate "m", or strong "s".

Fig. 4 displays a molecule of Cu(L-arg)$_2$SO$_4$ including the chemical path P_{AB} connecting a copper ion in an A site with two neighbors copper ions type B at 5.908 Å. This chemical path is composed of two branches. One contains an equatorial–apical carboxylate bond of the *syn–anti* type, –Cu$_A$–O2$_{ap}$–C2–O1$_{eq}$–Cu$_B$–, and has a total bond length of 7.133 Å. The other branch, –Cu$_A$–O1$_{eq}$–C2–O2···H–O1w$_{ap}$–Cu$_B$–, contains a weak hydrogen bond (#1, in Table 1) and has a total length of 9.781 Å. It will be clear that the second branch provides a much weaker contribution to the interaction between A and B-type copper neighbors than the first branch, and we neglect its contribution. A copper type A is connected to two copper neighbors type B through symmetry related paths P_{AB}.

Fig. 5 shows the two different chemical paths connecting a Cu$_A$ ion to two Cu$_C$ neighbors. One of them, –Cu$_A$–N5$_{eq}$–H···O5···H–N3–C6–N2–C5–C4–AC3–C1–N1$_{eq}$–

Table 1
Distances and angles (in Å and °) for the H-bonds which are relevant for the exchange paths between neighbor Cu ions in Cu(L-arg)$_2$SO$_4$ were obtained by complete data tables deposited by Ohata et al. [22] at Cambridge Crystallographic Data Centre

H-bond #	X–H···A bond	Length	X–H length	H···A length	Total length	Angle	Type
1	O1w$_{ap}$–H···O2	2.884	0.891	2.711	3.602	92.05	w
2	N5–H···O5	2.878	0.899	2.345	3.244	117.96	w
3	O3w–H···O5	2.925	1.147	1.985	3.132	136.45	w
4	N7–H···O3w	3.050	0.900	2.165	3.065	167.75	m
5	N3–H···O5	2.915	0.900	2.046	2.946	162.04	m
6	O3w–H···O5w	2.812	0.905	1.916	2.821	170.08	s
7	N8–H···O5w	2.924	0.900	2.045	2.945	165.01	m
8	N8–H···O4	2.886	0.899	2.048	2.947	154.66	m
9	O5w–H···O8A	2.873	1.148	2.183	3.331	115.65	m
10	O4w–H···O8A	2.725	1.041	1.813	2.854	143.97	m
11	O4w–H···O4	2.715	0.854	1.865	2.719	173.52	m
12	N2–H···O7A	2.945	0.901	2.155	3.056	145.95	m
13	O2w–H···O6A	2.960	0.879	2.714	3.593	97.49	w
14	O2w–H···O2	2.780	0.962	1.871	2.833	156.55	m

The strength of these bonds are characterized as s = strong, m = moderate and w = weak, according the definitions of Steiner [26].

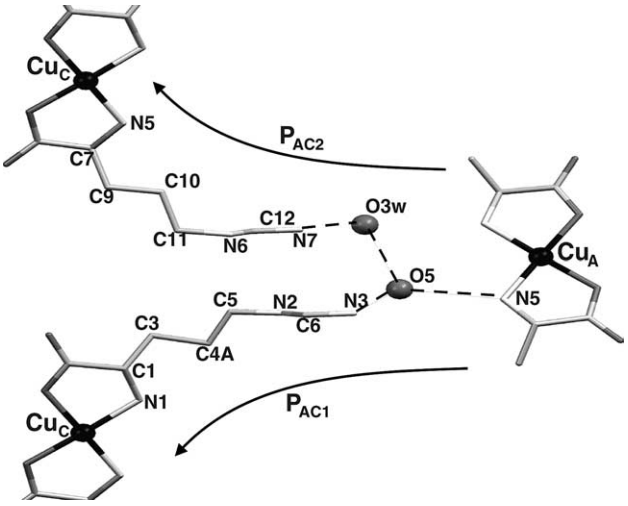

Fig. 5. Chemical paths connecting copper ions A and C. H-bonds are indicated with dashed lines. Hydrogen atoms were omitted for clarity.

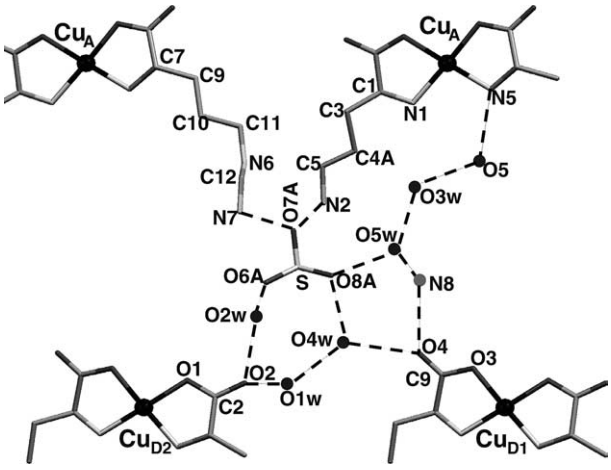

Fig. 6. Chemical paths connecting copper ions A and D. H-bonds are indicated with dashed lines. Hydrogen atoms were omitted for clarity.

Cu_C, called P_{AC_1}, connects coppers at 15.684 Å, contains 12 diamagnetic atoms, and has a total length of 19.789 Å. It includes a sequence of two H-bonds, #2 (w) and #5 (m), involving N5eq from the A molecule, N3 from a guanidinium group of the neighbor molecule and O5 from a sulphate group that bridges the two molecules. The other path, $–Cu_A–N5_{eq}–H\cdots O5\cdots H–O3w\cdots H–N7–C12–N6–C11–C10–C9–C7–N5_{eq}–Cu_C$, called P_{AC_2} connects coppers at 14.087 Å, has 14 atoms and a total length $d = 22.926$ Å. The path P_{AC_2} contains a sequence of three H-bonds, #2 (w), #3 (w) and #4 (m), involving O3w from a water molecule, O5 from a sulphate group, $N5_{eq}$ and N7. Because of the shorter length, the smaller number of atoms and particularly, because the smaller number of H–bonds, one may assume that P_{AC_1} supports an interaction stronger than P_{AC_2}.

The connections between Cu_A ions and Cu_D neighbors are shown in Fig. 6. The path P_{AD_1}, connecting coppers at 14.059 Å, is made of two branches. One branch is $–Cu_A–N5–H\cdots O5\cdots H–O3w–H\cdots O5w\cdots H–N8–H\cdots O4–C9–O3–Cu_D$, contains 13 diamagnetic atoms including a sequence of 5 H bonds #2 (w), #3 (w), #6 (s), #7 (m), and #8 (m), and has a total bond distance $d = 20.827$ Å. The other branch, $–Cu_A–N5–H\cdots O5\cdots H–O3w–H\cdots O5wH\cdots O8A\cdots H–O4wH\cdots O4–C9–O3–Cu_D$, has a total length $d = 23.350$ Å, and contains 17 diamagnetic atoms including 6 H-bonds, #2 (w), #3 (w), #6 (w), #9 (s), #10 (m), #11 (m). The path P_{AD_2}, $–Cu_A–N1–C1–C3–C4A–C5–N2–H\cdots O7A–S–O6A\cdots H–O2w\cdots O2–C2–O1–Cu_D$, connects copper ions at 17.786 Å, has a total length 26.166 Å and contains 12 diamagnetic atoms including three H–bonds, #12 (m), #13 (w) and #14 (m). A copper type A is connected to two coppers type D through paths P_{AD_1} and to other two coppers type D through paths type P_{AD_2}.

From this structural analysis it is clear that the bond paths connecting neighbor A and B type coppers are much stronger than the bond paths connecting a copper ion type A and neighbor copper ions types C and D. Consequently, the magnitude $|J_{AB}|$ of the exchange interaction between these Cu(II) ions is expected to be much larger than the exchange interactions $|J_{AC}|$ and $|J_{AD}|$. This result is important to interpret the EPR data. Also, assuming that H-bonds reduce the strength of the chemical path when compared with sigma bonds, one expects that the contribution to the interaction between A and B-type copper neighbors is dominated by the equatorial–apical carboxylate bridge.

In comparing the paths connecting copper atoms in sites A with neighbor copper atoms in sites C and D, we also assume that longer paths are weaker, and also that the larger is the number of H-bonds in the path, the weaker is its strength. With these two simple qualitative assumptions we conclude that the chemical paths connecting neighbor copper ions type A and C are stronger than those connecting neighbor coppers types A and D. This qualitative analysis indicates that $|J_{AC}| > |J_{AD}|$, as discussed further in the conclusions of this work.

4. Theoretical background

The angular variation of the position and line width of the EPR spectra of a single crystal of $Cu(L\text{-arg})_2SO_4$ is described by the Hamiltonian [18,27]:

$$\boldsymbol{H} = \boldsymbol{H}_z + \boldsymbol{H}_{ex}, \tag{1}$$

where the Zeeman contribution,

$$\boldsymbol{H}_z = \sum_i [\mu_B \mathbf{S}_{Ai} \cdot \boldsymbol{g}_A \cdot \boldsymbol{B} + \mu_B \mathbf{S}_{Bi} \cdot \boldsymbol{g}_B \cdot \boldsymbol{B} + \mu_B \mathbf{S}_{Ci} \cdot \boldsymbol{g}_C \cdot \boldsymbol{B} + \mu_B \mathbf{S}_{Di} \cdot \boldsymbol{g}_D \cdot \boldsymbol{B}], \tag{2}$$

is summed over all unit cells i of the crystal. μ_B is the Bohr magneton and $\boldsymbol{g}_\alpha$ ($\alpha = A, B, C, D$) are the symmetry

related molecular g-tensors corresponding to copper ions in the rotated crystal sites A, B, C, D, defined before. According to the space symmetry of Cu(L-arg)$_2$-SO$_4$, one expects four symmetry related EPR resonances corresponding to the four sites, for a general orientation of the applied field $\boldsymbol{B}$. Two resonances are expected when the magnetic field is within one of the crystal planes, where the g-factors are equal by pairs ($g_A = g_B$ and $g_C = g_D$ in the ab plane, $g_A = g_C$ and $g_B = g_D$ in the ac plane, and $g_A = g_D$ and $g_B = g_C$ in the bc plane). Only one resonance is expected when the magnetic field is along the crystal axes (see Section 5 for this space group in [28]).

The second term in Eq. (1):

$$\boldsymbol{H}_{ex} = \sum_{i,j} \boldsymbol{H}_{ex}^{i,j} = -\sum_{i,j} J_{ij} \mathbf{S}_i \mathbf{S}_j, \tag{3}$$

is the Heisenberg exchange interaction, where J_{ij} is the exchange parameter and i, j label different copper sites. According to Anderson's theory of the exchange narrowing process, when $|J_{ij}|$ is larger than the difference between the Zeeman energies corresponding to copper sites i and j, their resonances collapse to a single one [29]. Magnetic dipolar interactions, which are expected to have smaller magnitudes than the predominant exchange couplings J_{AB} are averaged out by the exchange and not considered here.

In previous papers we reported procedures to evaluate the exchange parameters J from the EPR data [18,27]. $\boldsymbol{H}_z$ of Eq. (2) is decomposed in an average contribution $\boldsymbol{H}_{z0}$, and a residual Zeeman term $\boldsymbol{H}_{z1}$. According to the structural discussion given above and considering interactions between nearest neighbor copper ions, it is $|J_{AB}| \gg |J_{AC}|$ and $|J_{AB}| \gg |J_{AD}|$. [1] Thus, it is convenient to decompose $\boldsymbol{H}_z$ in two contributions:

$$\boldsymbol{H}_z = \boldsymbol{H}_{z0} + \boldsymbol{H}_{z1}, \tag{4}$$

where $\boldsymbol{H}_{z0}$ is the main Zeeman contribution:

$$\boldsymbol{H}_{z0} = \mu_B(\mathbf{S}_A + \mathbf{S}_B) \cdot \frac{\boldsymbol{g}_A + \boldsymbol{g}_B}{2} \cdot B^{\blacksquare} + \mu_B(\mathbf{S}_C + \mathbf{S}_D) \cdot \frac{\boldsymbol{g}_C + \boldsymbol{g}_D}{2} \cdot \boldsymbol{B}^{\blacksquare}, \tag{5}$$

and $\boldsymbol{H}_{z1}$ is a smaller residual contribution:

$$\boldsymbol{H}_{z1} = \mu_B(\mathbf{S}_A - \mathbf{S}_B) \cdot \frac{\boldsymbol{g}_A - \boldsymbol{g}_B}{2} \cdot \boldsymbol{B} + \mu_B(\mathbf{S}_C - \mathbf{S}_D) \cdot \frac{\boldsymbol{g}_C - \boldsymbol{g}_D}{2} \cdot \boldsymbol{B}^{\blacksquare}. \tag{6}$$

The exchange interaction of Eq. (3) is decomposed in three contributions. A first one, $\boldsymbol{H}_{ex}$ (1), contains the largest terms corresponding to the interaction between pairs of copper sites AB and C–D. The other two contributions, $\boldsymbol{H}_{ex}(2)$ and $\boldsymbol{H}_{ex}(3)$, contain the exchange interactions between pairs of copper sites AC and BD, and AD and BC, respectively. Their contributions are smaller than that of $\boldsymbol{H}_{ex}(1)$.

Since the residual Zeeman interaction $\boldsymbol{H}_{z1}$ (Eq. (6)) does not commute with the exchange contribution $\boldsymbol{H}_{ex}(1)$, $\boldsymbol{H}_{z1}$ is modulated in time, and averaged to zero. Instead, $\boldsymbol{H}_{ex}(1)$ commutes with $\boldsymbol{H}_{z0}$ and does not change it. Thus, for exchange couplings J_{AB} (J_{CD}) large compared with the difference between the Zeeman terms of the A and B sites ($\boldsymbol{H}_{z1}$), one observes two resonances with g-tensors $\boldsymbol{g_1} = \frac{g_B + g_B}{2}$ and $\boldsymbol{g_2} = \frac{g_C + g_D}{2}$, except when $\boldsymbol{B}$ is in the planes ac and bc, when these resonances collapse to one because of the crystal symmetry. The EPR experiments verify this result, proving that $|J_{AB}| \gg |J_{AC}|$ and $|J_{AB}| \gg |J_{AD}|$, as suggested by the structural analysis. The components of the "crystal" g-tensors $\boldsymbol{g}_1$ and $\boldsymbol{g}_2$ (see Section 5) can be evaluated from the data. The "molecular" g-tensors, $\boldsymbol{g_A}, \ldots, \boldsymbol{g_D}$ introduced in Eq. (2) can be evaluated from these crystal $\boldsymbol{g}$ tensors making reasonable assumptions (see following section).

The smaller contributions $\boldsymbol{H}_{ex}(2)$ and $\boldsymbol{H}_{ex}(3)$ to the exchange interaction do not commute with $\boldsymbol{H}_{z0}$ of Eq. (5), and thus $\boldsymbol{H}_{z0}$ is modulated in time. Since the magnitudes of $\boldsymbol{H}_{ex}(2)$ and $\boldsymbol{H}_{ex}(3)$ are small, they collapse the resonances with g factors g_1 and g_2 in the ab plane only for magnetic field orientations close to the a and b axes, where $\Delta g = |g_1 - g_2|$ is small. In the range of orientations of $\boldsymbol{B}$ close to the axes in the ab plane (collapsed region) the line width $\Delta B_{pp}(\theta, \varphi)$ carries information about the weak exchange couplings J_{AC} and J_{AD}. To extract this information from the experimental results we use methods described previously [18,27,30,31]. The result for $\Delta B_{pp}(\theta, \varphi)$ in the collapsed region of the ab plane is:

$$\Delta B_{pp}(\theta, \varphi) = \sqrt{\frac{2\pi}{3}} \frac{\omega_0^2 \hbar}{g \mu_B} \frac{1}{\omega_{ex}^{(3)}} \frac{(\boldsymbol{h} \cdot \boldsymbol{g} \cdot \boldsymbol{G}_3 \cdot \boldsymbol{h})^2}{g^4(\theta, \varphi)} + \Delta B_{pp}(0), \tag{7}$$

with $\boldsymbol{G}_3 = 1/2\,(\boldsymbol{g_A} - \boldsymbol{g_C})$, which depends on the square of the microwave frequency ω_0. In Eq. (7) $\Delta B_{pp}(0)$ is the residual line width due to other sources, observed when the magnetic field is parallel to the crystalline axes and $\omega_{ex}^{(3)}$ is the exchange frequency between non-equivalent neighbor copper ions, given in our problem by:

$$(\omega_{ex}^{(3)})^2 = \frac{1}{\hbar^2}\left[\left(J^{(A,C)}\right)^2 + 2\left(J^{(A,D)}\right)^2\right], \tag{8}$$

where the factor 2 indicates the number of Cu_D ions which are nearest neighbor of a Cu_A ion. Only one Cu_C nearest neighbour to a Cu_A exists, and this is considered in Eq. (8) [18]. In Eq. (7), $\boldsymbol{h} = \mathbf{B}/|\mathbf{B}| = (\sin\theta\cos\varphi, \sin\theta\sin\varphi, \cos\theta)$ defines the magnetic field orientation in the $xyz = abc$ system of axes and $\boldsymbol{h} \cdot \boldsymbol{g} \cdot \boldsymbol{G_3} \cdot \boldsymbol{h}$, is proportional to one non-diagonal matrix element of the *molecular* $\boldsymbol{g}$-tensors ($\boldsymbol{g_A}, \ldots, \boldsymbol{g_D}$) in the crystal axes system [18]:

[1] For symmetry considerations $J_{AB} = J_{CD}$ $J_{AC} = J_{BD}$ and $J_{AD} = J_{BC}$ which results in other similar conditions.

$$\frac{(\boldsymbol{h}\cdot\boldsymbol{g}\cdot\boldsymbol{G_3}\cdot\boldsymbol{h})^2}{g^2(\theta,\varphi)} \simeq \left\{\boldsymbol{h}\cdot\frac{1}{2}(\boldsymbol{g}_{\mathrm{A}}-\boldsymbol{g}_{\mathrm{C}})\cdot\boldsymbol{h}\right\}^2 = g_{ab}\sin^2\theta\cos^2\theta. \quad (9)$$

From the fit of Eqs. (7)–(9) to the line width data in the collapsed region of the *ab* plane, the exchange frequency of Eq. (8) can be evaluated. Information about the magnitudes of the exchange interactions J_{AC} and J_{AD} is provided by Eq. (8).

5. Analysis of the EPR results

5.1. The crystal and molecular g-tensors

The components of the squared crystalline $\boldsymbol{g}$-tensors, $\boldsymbol{g}_1^2$ and $\boldsymbol{g}_2^2$, obtained by least-squares fittings of the function $g^2(\theta,\varphi) = \boldsymbol{h}\cdot\boldsymbol{g}\cdot\boldsymbol{g}\cdot\boldsymbol{h}$ to the g^2-values for the two lines of the spectra, at each microwave frequency, are given in Table 2 together with their eigenvalues and eigenvectors. Fig. 2 includes as solid lines the angular variations of $g_1^2(\theta,\varphi)$ and $g_2^2(\theta,\varphi)$ at Q-band calculated with the components of the tensors given in Table 2. These curves are in good agreement with the experimental data at 34.1 GHz. Similar agreement is found at X band (not shown).

In order to evaluate the molecular $\boldsymbol{g}_i$-tensors (i = A, B, C, D) of the individual copper ions in Cu(L-arg)$_2\cdot$SO$_4$ we followed a procedure described previously [32–34]. Since the coordination around the copper ion is approximately square planar, we assumed axially symmetric molecular $\boldsymbol{g}$-tensors with θ_{m} and φ_{m} being the polar and azimuthal angles corresponding to the direction along which $g_\parallel$ is measured for copper ions in site A. With this assumption we obtained from the single crystal results the values of $g_\parallel$, $g_\perp$, θ_{m}, φ_{m} and the angle 2α between the apical directions corresponding to copper sites A and C (or B and D) included in Table 2. The angular values are in good agreement with those obtained from the crystal structure (also included in Table 2), thus supporting the assumptions made in the calculation. The values of $g_\parallel$ and $g_\perp$ are similar to those reported by Ohata et al. [22] in frozen solution ($g_\parallel = 2.26$, $g_\perp = 2.08$), indicating similar ligand environments for the copper ions in solution and in the solid.

Table 2
Components of the crystal $\boldsymbol{g}^2$ tensors obtained by fitting the function $g^2 = (\boldsymbol{h}\cdot\boldsymbol{g}\cdot\boldsymbol{g}\cdot\boldsymbol{h})$ to the experimental data in Fig. 3

	9.8 GHz	34.1 GHz
$(g^2)_{xx}$	4.2473(8)	4.2760(9)
$(g^2)_{yy}$	4.2995(8)	4.3336(8)
$(g^2)_{zz}$	5.0016(9)	4.9982(9)
$(g^2)_{xy}$	0.000(1)	0.0238(6)
$(g^2)_{xz}$	0.009(1)	0.0242(9)
$(g^2)_{yz}$	0.006(1)	0.0060(9)
$\boldsymbol{a}_1$	(0.012, 0.009, 0.999)	(0.034, 0.010, 0.999)
$\boldsymbol{a}_2$	(0.999, –0.012, –0.012)	(0.942, ∓0.333, –0.028)
$\boldsymbol{a}_3$	(0.012, 0.999, –0.009)	(0.333, ±0.943, –0.021)
$(g^2)_1$	5.0018(8)	4.9991(9)
$(g^2)_2$	4.2472(8)	4.2668(9)
$(g^2)_3$	4.2994(8)	4.3419(8)
$g_\perp$	2.0608(8)	2.0656(5)
$g_\parallel$	2.2480(6)	2.2526(5)
2α	150.2^0	144.5^0
θ_{m}	163.3^0	163.5^0
φ_{m}	9.1^0	9.0^0
$2\alpha^{\mathrm{crys}}$	147.9^0	
$\theta_{\mathrm{m}}^{\mathrm{crys}}$	162.9^0	
$\varphi_{\mathrm{m}}^{\mathrm{crys}}$	9.1^0	

$(g^2)_1$, $(g^2)_2$, $(g^2)_3$ and $\boldsymbol{a}_1$, $\boldsymbol{a}_2$, $\boldsymbol{a}_3$ are the eigenvalues and eigenvectors. $g_\perp$ and $g_\parallel$ were calculated assuming axial symmetry for the molecular g tensor of the copper ions.
The angle 2α between the normals $\mathbf{n}_{\mathrm{A}}$ and $\mathbf{n}_{\mathrm{C}}$ to the planes of ligands to copper ions in sites A and C in the *abc* coordinate system calculated from our EPR data and from the crystallographic results [22] are included.

The powder spectra measured at X- and Q-bands (not shown) was simulated using the program Simfonia (Bruker Instruments) using the values of the g-tensor and the angular variation of the line with observed in the single crystals. A very good agreement obtained between simulations and data at both microwave frequencies reflects the quality of the single crystal study.

The fact that a single resonance is observed in the *ac* and *bc* planes indicates that the exchange interaction J_{AB} collapses the resonances corresponding to the magnetically nonequivalent copper ions A and B. This observation indicates that $|J_{\mathrm{AB}}| \geqslant |\Delta g_{\mathrm{AB}}\mu_{\mathrm{B}}B|$ and, considering the values of the molecular g-tensors and the orientation of A and B molecules in the crystal, we obtain $|J_1| = |J_{\mathrm{AB}}| \geqslant 0.9$ K.

5.2. The EPR line width

Fig. 3 displays the angular dependence of the line width $\Delta B_{\mathrm{pp}}(\theta,\varphi)$ at 34.1 GHz, in the crystalline planes *ab*, *ca* and *cb*. The symbols represent the experimental data and the solid line close to the *b*-axis were calculated as explained before. Using Eqs. (5)–(7), the values of the non-diagonal components of the molecular $\boldsymbol{g}$-tensors, and the line width results in Fig. 3, we calculated $\hbar\omega_{\mathrm{ex}}^{(3)}/k_{\mathrm{B}} = 0.016(2)$ K from the data in the *ab* plane. Considering Eq. (8) and the structural discussion given above, this result allows to evaluate the smaller exchange interaction $|J_2|/k_{\mathrm{B}} = 0.009(2)$ K, that according the discussion in the structural section is assigned to $|J_{\mathrm{AC}}|$. The EPR method does not allow obtaining the sign of the interaction.

6. Discussion and conclusions

The values of the components of the g-tensor at two microwave frequencies are similar, and the

differences observed can be attributed to small non-secular contributions arising from $\boldsymbol{H}_{z1}$ (Eq. (6)). Our values of the g-factors obtained from the single crystal data are more accurate than those from [22] obtained from simulations of the spectra of powder samples and we also provide the eigenvectors of the g-tensor. The eigenvalues of the g-tensor given in Table 2, indicate a $d(x^2 - y^2)$ for the ground state orbital [35] of Cu in Cu(L-arg)$_2$SO$_4$, as already observed by Ohata et al. [22].

From our experimental results we can not evaluate the exchange interaction J_{AA} between equally oriented nearest neighbor copper ions along the a axis separated by 13.152 Å because this interaction commutes with the Zeeman interaction and does not affect the EPR spectra.

Considering that in the present case d(Cu–O$_{ap}$) = 2.461 Å, the lower limit $|J_{AB}|/k_B \geqslant 0.9$ K estimated above for the exchange coupling between neighbor coppers in A and B sites at $d = 5.908$ Å from the collapse of the resonances in the ac and bc planes, compares well with the prediction $|J_{AB}|/k_B \approx 0.9$ K of the model proposed by Levstein and Calvo [36] for the magnitude of the exchange interaction transmitted by equatorial–apical carboxylate bonds. This prediction is also supported by the results of specific heat measurements at very low temperatures [37,38].

From the angular dependence of the line width displayed in Fig. 3b, we evaluated the parameter $|J_2|/k_B = 0.009(2)$ K which according to the structural discussion is associated with the chemical path P_{AC_1} shown in Fig. 5, e.g., $|J_{AC}|/k_B = 0.009(2)$ K. The length of this path is 19.789 Å and it includes 9 σ-bonds and 2 H-bonds involving an oxygen atom from the sulphate anion.

Exchange interactions between copper ions connected by *syn–anti* carboxylate bridges have been evaluated by Colacio et al. [39] and Costa-Filho et al. [30] using magnetic measurements in different compounds. Using the definition of J given in Eq. (3), they reported ferromagnetic interactions with magnitudes values $J/k_B = 4.8$ and 3.9 K, respectively. These values are larger than that reported here for the interaction transmitted through the path P_{AB} in Cu(L-arg)$_2$SO$_4$, because the equatorial–equatorial carboxylate path connecting copper ions in the compounds studied in [30,39] is stronger than the equatorial–apical carboxylate bond occurrying in Cu(L-arg)$_2$SO$_4$.

Hoffmann et al. [17] studied the dependence of the weak superexchange interaction with the length of the chemical paths in copper (II) compounds. Calvo et al. [40] performed a similar analysis of magnitudes of exchange interactions between unpaired spins in protein structures. In both cases the results were analyzed considering a dependence of $|J|$ with distance (d) given by the exponential function,

$$|J| \propto \exp(-\beta_J d),$$

where, according to Hoffmann et al. [17], $\beta_J = 0.33$ Å^{-1}, and according to Calvo et al., $\beta_J = 0.66$ Å^{-1}. Considering the values of $|J_{AB}|$ and $|J_{AC}|$ estimated here in Cu(L-arg)$_2$SO$_4$, and the distances between A and B, and A and C copper neighbors, we estimate $\beta_J = 0.47$ Å^{-1}, in very good agreement with these previous values. These estimates do not consider specific details of the paths and are useful to obtain crude predictions of the magnitude of the interactions (see [40]).

An exchange interaction between the reduced quinone acceptors Q_A^- and Q_B^- in the biradical $Q_A^- Q_B^-$ of the photosynthetic reaction center protein from the bacterium *Rb. Sphaeroides* was recently evaluated [13a,b]. The magnitude of the coupling measured by EPR measurements at 326 GHz, $|J/k_B| = 0.0039(1)$ K [13b], is very similar to the value obtained for J_2 in the model system studied here. According to the structural data for the reaction center [41], the distance between the ring centers of the two quinone acceptors is 17.2 Å and the chemical path connecting the quinones (shown in Fig. 9 of reference [13a]) contains 13 atoms, including two hydrogen bonds. It is the path for the electron transfer between the two quinones during the photosynthetic cycle. The similarity of the magnitudes of the exchange interactions measured in a model system and in an electron transfer protein which are supported by similar paths is an important result of our work. It indicates that it is valid using model systems to estimate exchange interactions between unpaired spins (metal or radical ions) transmitted along long chemical paths containing sigma and H-bonds. Thus, more systematic measurements of exchange interactions in model systems are needed. Also, theoretical work treating with greater detail the relationship between exchange interactions and the matrix elements for electron transfer supported by equal chemical paths [13] would be important to improve calculations of electron transfer rates. As the weakest segments of the chemical paths are the H-bonds one should progress experimentally and theoretically in the understanding of exchange interactions supported by these bonds.

In conclusion, this work provides a detailed single crystal EPR study of electronic properties and magneto-structural correlations for the ternary copper compound Cu(L–arg)$_2$SO$_4$. We evaluate the principal values and directions of the g-tensor of the copper ion and, most important, estimate the magnitudes $|J_1|/k_B \approx 0.9$ K and $|J_2|/k_B = 0.009$ K of the exchange interactions between nearest neighbor copper ions and assign them to specific diamagnetic chemical paths in the structure of Cu(L-arg)$_2$SO$_4$. These results were successfully compared with measurements in other compounds and in a relevant electron transfer protein.

They proof the value of EPR to selectively measure extremely weak exchange interactions ($0.0003 < |J/k_B| < 1$ K).

Acknowledgements

The authors acknowledge financial support from Conselho Nacional de Desenvolvimento Científico e Tecnológico (CNPq) and Fundação de Apoio à Pesquisa da Universidade Federal de Goiás (FUNAPE) in Brazil, and grants CAI+D from Universidad Nacional del Litoral and from Fundación Antorchas in Argentina. RC is a member of CONICET.

References

[1] S.J. Lippard, J.M. Berg, Principles of Bioinorganic Chemistry, University Science Books, Mill Valley, CA, 1994.
[2] G.A. Jeffrey, An Introduction to Hydrogen Bonding, Oxford University Press, New York, 1997.
[3] G.A. Jeffrey, W. Saenger, H-Bonding in Biological Molecules, Springer, Berlin, 1991.
[4] B.E. Fisher, H.J. Sigel, J. Am. Chem. Soc. 102 (1980) 2998–3008.
[5] T. Sugimori, K. Shibakawa, H. Masuda, A. Odani, O. Yamauchi, Inorg. Chem. 32 (1993) 4951–4959.
[6] D.A. Dougherty, Science 271 (1996) 163–168.
[7] J.C. Ma, D.A. Dougherty, Chem. Rev. 97 (1997) 1303–1324.
[8] M.F. Perutz, Phil. Trans. Roy. Soc. A 345 (1993) 105–112.
[9] M. Nishio, M. Hirota, Y. Umezawa, The CH–π interactions, Wiley, New York, 1998.
[10] O. Kahn, Molecular Magnetism, VCH, New York, 1993.
[11] M.Y. Okamura, D.R. Fredkin, R.A. Isaacson, G. Feher, in: B. Chance, D.C. DeVault, H. Frauenfelder, R.A. Marcus, J.R. Schriefer, N. Suttin (Eds.), Tunneling in Biological Systems, Academic Press, New York, 1979, pp. 729–743.
[12] D. DeVault, Quantum Mechanical Tunneling in Biological Systems, Cambridge University Press, Cambridge, 1984, pp. 118–121.
[13] (a) R. Calvo, E.C. Abresch, W. Bittl, G. Feher, W. Hofbauer, R.A. Isaacson, W. Lubitz, M.Y. Okamura, M.L. Paddock, J. Am. Chem. Soc. 122 (2000) 7327–7341;
(b) R. Calvo, R.A. Isaacson, M.L. Paddock, E.C. Abresch, M.Y. Okamura, A.L. Maniero, L.C. Brunel, G. Feher, J. Phys. Chem. B 105 (2001) 4053–4057.
[14] Y. Kobori, T. Yago, K. Akiyama, T. Tero-Kubota, H. Sato, F. Hirata, J.R. Norris, J. Phys. Chem. B 108 (2004) 10226–10240.
[15] A. Abragam, B. Bleaney, Electron Paramagnetic Resonance of Transition Ions, Clarendon Press, Oxford, 1970.
[16] A. Bencini, D. Gatteschi, Electron Paramagnetic Resonance of Exchange Coupled Systems, Springer, Berlin, 1990.
[17] S.K. Hoffmann, W. Hilczer, J. Goslar, Appl. Magn. Reson. 7 (1994) 289–321.
[18] M.C.G. Passeggi, R. Calvo, J. Magn. Reson. A 114 (1995) 1–11.
[19] H.C. Freeman, in: L. Eichhorn (Ed.), Inorganic Biochemistry, vol. 1, Elsevier, Amsterdam, 1973 (Chapter 4).
[20] O. Yamauchi, A. Odani, M. Takani, J. Chem. Soc., Dalton. Trans. (2002) 3411–3421.
[21] N. Ohata, H. Masuda, O. Yamauchi, Inorg. Chim. Acta 286 (1999) 37–45.
[22] N. Ohata, H. Masuda, O. Yamauchi, Inorg. Chim. Acta 300-302 (2000) 749–761, Complete structural data tables is deposited at the Cambridge Crystallographic Data Centre under number 137772.
[23] H. Masuda, A. Odani, T. Yamazaki, T. Yahima, O. Yamauchi, Inorg. Chem. 32 (1993) 1111–1118.
[24] N. Ohata, H. Masuda, O. Yamauchi, Angew. Chem., Int. Ed. Eng. 35 (1996) 531–532.
[25] T. Hahn (Ed.), International Tables for X-Ray Crystallography, Reidel, 1983.
[26] T. Steiner, Angew. Chem., Int. Ed. 41 (2002) 48–76.
[27] C.D. Brondino, N.M.C. Casado, M.C.G. Passeggi, R. Calvo, Inorg. Chem. 32 (1993) 2078–2084.
[28] R. Calvo, S.B. Oseroff, H.C. Abache, J. Chem. Phys. 72 (1980) 760–767.
[29] P.W. Anderson, J. Phys. Soc. Jpn. 9 (1954) 316–339.
[30] A.J. Costa–Filho, O.R. Nascimento, L. Ghivelder, R. Calvo, J. Phys. Chem. B 105 (2001) 5035–5047.
[31] A.J. Costa–Filho, O.R. Nascimento, R. Calvo, J. Phys. Chem. B 108 (2004) 9549–9555.
[32] H. Abe, K. Ono, J. Phys. Soc. Jpn. 11 (1956) 947–956.
[33] D.E. Billing, B.J. Hathaway, J. Chem. Phys. 50 (1969) 1476–1477.
[34] R. Calvo, M. Mesa, Phys. Rev. B 28 (1983) 1244–1248.
[35] H.J. Zweiger, G.W. Pratt, Magnetic Interactions in Solids, Oxford University Press, London, 1973.
[36] P.R. Levstein, R. Calvo, Inorg. Chem. 29 (1990) 1581–1583.
[37] M.L. Siqueira, R.E. Rapp, R. Calvo, Phys. Rev. B 48 (1993) 3257–3263.
[38] R.E. Rapp, E.P. de Souza, H. Godfrin, R. Calvo, J. Phys. Condens. Matter 7 (1995) 9595–9606.
[39] E. Colacio, J.M. Dominguez-Vera, J.P. Costes, R. Kivekäs, J.P. Laurent, J. Ruiz, M. Sundberg, Inorg. Chem. 31 (1992) 774–778.
[40] R. Calvo, R.A. Isaacson, E.C. Abresch, M.Y. Okamura, G. Feher, Biophys. J. 83 (2002) 2440–2456.
[41] M.H.B. Stowell, T.M. Phillips, D.C. Rees, S.M. Soltis, E.C. Abresch, G. Feher, Science 276 (1997) 812–816.